

# Turbidity-discharge hysteresis in a meso-scale catchment: The importance of intermediate scale events

Emma E. Lannergård  | Jens Fölster  | Martyn N. Futter 

Department of Aquatic Sciences and Assessment, Swedish University of Agricultural Sciences, Uppsala, Sweden

## Correspondence

Emma E. Lannergård, Department of Aquatic Sciences and Assessment, Swedish University of Agricultural Sciences, Uppsala, Sweden.  
Email: emma.lannergard@slu.se

## Funding information

Svenska Forskningsrådet Formas, Grant/Award Numbers: 2015-1518, 2017-00029

## Abstract

In-situ sensors for riverine water quality monitoring are a powerful tool to describe temporal variations when efficient and informative analyses are applied to the large quantities of data collected. Concentration-discharge hysteresis patterns observed during storm events give insights into headwater catchment processes. However, the applicability of this approach to larger catchments is less well known. Here, we evaluate the potential for high-frequency turbidity-discharge ( $Q$ ) hysteresis patterns to give insights into processes operating in a meso-scale ( $722 \text{ km}^2$ ) northern mixed land use catchment. As existing event identification methods did not work, we developed a new, objective method based on hydrograph characteristics and identified 76 events for further analysis. Qualitative event analysis identified three recurring patterns. Events with low mean  $Q$  ( $\leq 2 \text{ m}^3/\text{s}$ ) often showed short-term, quasi-periodic turbidity variation, to a large extent disconnected from  $Q$  variation. High max  $Q$  events ( $\geq 15 \text{ m}^3/\text{s}$ ) were often associated with spring flood or snowmelt, and showed a disconnection between turbidity and  $Q$ . Intermediate  $Q$  events (mean  $Q$ :  $2\text{--}11 \text{ m}^3/\text{s}$ ) were the most informative when applying hysteresis indexes, since changes in turbidity and  $Q$  were actually connected. Hysteresis indexes could be calculated on a subset of 60 events, which showed heterogeneous responses: 38% had a clockwise response, 12% anticlockwise, 12% figure eight (clockwise-anticlockwise), 10% reverse figure eight (anticlockwise-clockwise) and 28% showed a complex response. Clockwise hysteresis responses were associated with the wetter winter and spring seasons. Generally, changes in  $Q$  and turbidity were small during anti-clockwise hysteresis events. Precipitation often influenced figure-eight patterns, while complex patterns often occurred during summer low flows. Analysis of intermediate  $Q$  events can improve process understanding of meso-scale catchments and possibly aid in choosing appropriate management actions for targeting a specific observed pattern.

## KEY WORDS

catchment processes, C-Q analysis, event identification, high frequency turbidity, hysteresis index, meso-scale

This is an open access article under the terms of the Creative Commons Attribution License, which permits use, distribution and reproduction in any medium, provided the original work is properly cited.

© 2021 The Authors. *Hydrological Processes* published by John Wiley & Sons Ltd.

## 1 | INTRODUCTION

Successful management of surface water quality is dependent on adequate and appropriate monitoring (Fölster et al., 2014). High-frequency (HF) measurements using, for example, in-situ sensors show great promise to monitor short-term temporal changes in water quality (e.g., Cassidy & Jordan, 2011; Coynel et al., 2004; Kirchner et al., 2004). Suspended sediment (and associated pollutants) are known to display high temporal variation in concentration (Bilotta & Brazier, 2008), which is why these parameters are especially important to monitor with a high frequency. To optimize mitigation and management action plans in catchments with varying pollutant sources we need to understand the processes and mechanisms that affect, for example, mobilization of total suspended solids (TSS) particulate phosphorus (PP) and other particle bound pollutants (Haddadchi & Hicks, 2020b; Sherriff et al., 2016).

Turbidity is a water quality parameter that can be easily monitored with in-situ sensors. It is a measure of cloudiness in the water, and can be used as a proxy for TSS and total phosphorus (TP) (Grayson et al., 1996; Lannergård et al., 2019; Skarbøvik & Roseth, 2015). Data from daily/sub-daily HF monitoring can provide more accurate transport calculations (e.g., annual sediment or phosphorus fluxes) since periods of peak concentrations are better characterized, compared to calculations based on lower resolution sampling (e.g., biweekly/monthly) (Defew et al., 2013; Johnes, 2007; Jones et al., 2012; Lannergård et al., 2019). Over the past decade, development of more robust sensors with better performance has increased their use in both research and monitoring (Rode et al., 2016; van Geer et al., 2016). The high volumes of data collected must be efficiently analysed and understood if we are to use HF sensors to better support environmental management.

One strategy to handle the large data volume is to restrict analyses to especially informative periods. High flow events transport large amounts of nutrients and sediment compared to the rest of the year (Kronvang & Bruhn, 1996). These events, which display a meaningful change in the hydrograph can be initiated by precipitation, often called storm events (Fovet et al., 2018; Jordan et al., 2007; Kronvang et al., 1999; Perks et al., 2015), or snowmelt (Lana-Renault et al., 2011; Langlois et al., 2005). Flow changes during the event activate mobilization processes (e.g., overland flow, erosion from bankside areas or within the stream) that influence surface water quality.

Concentrations (C) of both dissolved and particulate pollutants can display different responses to changes in flow (Q), for example, increase through mobilization, decrease through dilution, or show no net change (Rose et al., 2018). Evaluating simultaneous changes in C and Q has contributed to understanding the processes controlling transport of particulate (e.g., Walling, 1977; Walling & Webb, 1982) and dissolved substances (e.g., Seibert et al., 2009).

Evaluating differences in the temporal patterns of C and Q during events (hysteresis patterns) is a widely used approach to understanding more about catchment processes and hydrological pathways (Bieroza & Heathwaite, 2015; Bowes et al., 2005; Butturini et al., 2008; Evans & Davies, 1998; Fovet et al., 2018; Glover &

Johnson, 1974; Hashemi et al., 2020; Heathwaite & Bieroza, 2020; Rose et al., 2018; Walling & Foster, 1975). So-called “hysteresis loops” are often used to graphically represent such differences. The shape of these loops (slope, shape, rotational pattern) varies depending on the timing and magnitude of peaks in C and Q (Evans & Davies, 1998). The C-Q mismatch in time can be further analysed and different hysteresis patterns could, for example, give insight into dominant hydrological pathways during flow events (Evans & Davies, 1998; Rose et al., 2018), contributing source areas or source limitations (Outram et al., 2014; Williams, 1989). Hysteresis patterns are easier to see in events with single-peak hydrographs, compared with multi-peak hydrographs where patterns become complex very quickly.

Many different ways of describing hysteresis loops have been suggested, but most are variants on idealized fast (clockwise) or slow (anticlockwise) system responses (Evans & Davies, 1998; Haddadchi & Hicks, 2020b; Williams, 1989). These simple descriptions may be insufficiently specific for a satisfactory analysis of hysteretic behaviour during events (Butturini et al., 2008). Hysteresis patterns seen in actual data are often more complex and cannot readily be described only in terms of clockwise or anticlockwise loops (Haddadchi & Hicks, 2020b; Williams, 1989).

Therefore, quantitative indexes, based on a dimensionless quantification of the hysteresis loop, have been used to compare events in catchments of different sizes, morphology and hydrology (Lloyd et al., 2016). Lawler et al. (2006) developed an index that can be applied to hysteresis loops of all shapes based on the ratio of concentration on the rising and falling limb at the mid-point of the hydrograph. An improved hysteresis index calculated as the difference between concentrations on the rising and falling limb estimated for example, 1%, 5%, 10% or 25% increments of discharge was developed by Lloyd et al. (2016).

To understand processes and mechanisms operating in the catchment, it is necessary to connect hysteresis results to environmental conditions. There are, however, numerous underlying causes for temporal and spatial variations in hydrological and biogeochemical processes which in turn influence the shape of hysteresis loops, in this case describing the turbidity-Q relationship.

The character of the driving force (intensity/duration of precipitation, snowfall, snowmelt) causing the hydrological event is important for the C-Q relationship and is closely connected to different seasons, for example, frozen soils, snow cover, and antecedent moisture conditions (Eder et al., 2010). Hydrological pathways route the water and define hydrological connectivity, with wetter conditions leading to higher connectivity. The concept of hydrological connectivity encompasses multiple spatial scales, for example, vertically through the soil profile, laterally along hillslopes longitudinally along a stream (Ledesma et al., 2018). Connectivity further influences sources and availability of material and timing of delivery, which in turn influence hysteresis patterns (Evans & Davies, 1998). Hydrological connectivity can be affected by anthropogenic activities such as ditching (Kuglerová et al., 2017) or subsurface (tile) drainage (Gramlich et al., 2018). Tile drains generally increase soil infiltration capacity and

reduce overland flow as infiltrated water is rapidly transported laterally through the soil (Belmont et al., 2011); this implies higher base flows and lower Q peaks (Blann et al., 2009). However, delivery of material from soil, riparian areas and stream channels is affected by both the erosive agent and erodibility at the site (Verbrugge et al., 2017). Vegetation cover, land use and management practises all influence initial erosion, further transport and later remobilization of material (Verbrugge et al., 2017).

Hysteresis analysis has been used to understand processes and mechanisms under varying environmental conditions and land use (Bowes et al., 2005; Eder et al., 2010; Haddadchi & Hicks, 2020a; Lana-Renault et al., 2011; Lawler et al., 2006; Rose et al., 2018; Sherriff et al., 2016), and is potentially a way to convert HF data into insights supporting better management of surface water quality (e.g., Wenng et al., 2021). Hysteresis analysis studies conducted over longer time periods (Knapp et al., 2020) with all seasons represented are rare, as are studies in larger, meso-scale catchments ( $> 500 \text{ km}^2$ , Haddadchi & Hicks, 2020b). Larger catchments are more relevant for management purposes since this is the scale for monitoring efforts and management plans within, for example, the Water Framework Directive. However, the larger catchment scale could be a challenge both when applying the method and interpreting the results. A larger catchment implies that the water chemistry signal at the outlet integrates the range of different travel times needed for material to reach the monitoring station. With a complex catchment, the signal is also a mixture of responses from areas with different land use (e.g., forest, pasture and agriculture), lakes and sources of material for example river banks and in-stream sources.

The aim of this study was to use long-term HF data to connect turbidity variations during events to environmental variables and event characteristics, to better identify appropriate mitigation options for different seasons and flow conditions. Specifically, we evaluated the information in HF turbidity-Q hysteresis patterns for events extracted from a long-term time series (2012–2019) representing all seasons, in a meso-scale northern mixed land use catchment. Our hypothesis was that widely used metrics to describe HF turbidity-Q hysteresis patterns would give meaningful insight into catchment function and the techniques would be transferrable to other, similar meso-scale catchments. Based on previous studies our hypotheses were that hysteresis patterns vary depending on (1) high/low Q, (2) season and (3) event characteristics, for example, duration.

## 2 | DATA AND METHODS

### 2.1 | Site description

The study was conducted in Sävjaån, a river draining a mixed land use, meso-scale catchment ( $722 \text{ km}^2$ ) in east central Sweden. Forests are the dominant land cover type (71%); they are more common on the slightly higher elevation outwash till soils located in the north and east of the catchment (map in Figure S1). Agriculture and pasture (24%) is more prevalent on clay soils closer to the catchment outlet. The small urban area (2%) is part of the city of Uppsala (Swedish Meteorological

and Hydrological Institute, 2019). The few larger lakes (3%) are centrally located. The catchment is very flat, the highest point is 72 masl and the lowest 1 masl (National Land Survey, 2021).

The glacial/postglacial clay soils in the area have a clay content between 40% and 70% (Möller, 1993). In central Sweden, most agricultural areas located on clay soils are tile drained (Djordjevic, 2001). The most common crops are winter wheat and spring barley (Hansson et al., 2019). Animal husbandry is quite uncommon in the catchment, however, grazing in riparian areas is allowed and encouraged (Swedish Board of Agriculture, 2021).

Average annual precipitation is 639 mm and average annual runoff 189 mm (1981–2010) (Swedish Meteorological and Hydrological Institute, 2020). Mean annual temperature is  $6^\circ\text{C}$ , with a range of average daily temperatures between  $-27$  and  $+26^\circ\text{C}$  (1949–2017). During winter, streams are often ice covered for one or more months each year. Winter Q is sustained by groundwater and increasingly common winter rainfall and snowmelt events (Lannergård et al., 2020). Q is generally flashier during spring and autumn; summer Q is generally low (graphical presentation in Figure S2). High-frequency Q (HFQ) data (15 min) was available from the Swedish Meteorological and Hydrological Institute, which had monitored stage height at a flow weir close to the outlet of the catchment (Station ID 2243) until September 2020. Modelled flow velocity (described later) during 2012–2019 varied between 0.12 and 0.34 m/s which suggests a travel time in the hydrographic network between 2 and 5 days from the catchment headwaters to the monitoring station.

An in-situ sensor monitoring stream water chemistry every 10–15th min is located in Sävjaån close to the catchment outlet (2012–2016 YSI 6000MS, 2016–2019 YSI EXO2). Sensor maintenance, data quality control and treatment were described by Lannergård et al. (2019). Turbidity is generated by sediment, algal cells, colloidal humic substances, minerals and detrital organic matter (Bilotta & Brazier, 2008). Despite the fact that a good linear transfer function has previously been shown between turbidity and TSS and TP in Sävjaån ( $r^2 = 0.68$ ,  $r^2 = 0.64$  for the years 2012–2017) (Lannergård et al., 2019) all analyses reported here are restricted to turbidity and Q.

### 2.2 | Data analysis

#### 2.2.1 | Event identification

In previous literature, events have been defined with simple criteria, for example, when Q was larger than baseflow (Eder et al., 2010; Hashemi et al., 2020); by a certain increase from baseflow (Lana-Renault et al., 2011; Lloyd et al., 2016) and a subsequent return to baseflow (Eder et al., 2010; Lloyd et al., 2016). In Sherriff et al. (2016) events were defined as consecutive Q increase thresholds. Flow variation (e.g., an increase/decrease of more than 2 L/s) in combination with precipitation or previous precipitation (<5 mm in 24 h) was used in Fovet et al. (2018).

In our case, simpler event definitions were not applicable due to the complex nature of the hydrograph, for example, multiple Q peaks

and no return to baseflow (Figure S3). Start times for events were identified based on daily Q data satisfying the following criteria (Figure 1):

- I. A specific pattern in rising/falling limbs of the hydrograph was required (observation on the rising limb, two previous observations on the falling limb, next observation also on the rising limb).
- II. The inter-day increase in Q ( $x_1$ ) was  $>1.2\%$  (5th percentile of the distribution of Q increases during the years studied).
- III. Daily mean Q above  $0.1 \text{ m}^3/\text{s}$  ( $x_2$ , 10th percentile of Q data during the studied period).

The end of the event was also identified by three conditions:

- I. An event ended if a new event started and otherwise,
- II. Observed Q was less than the value predicted by a first order baseflow decay function based on Q at the start of the event and decreasing with  $0.1\%$  per day.
- III. When (II) was fulfilled but observed Q continued to decrease ( $x_3$ ), the event continued until there was no further decrease in Q.

The increase/decrease in daily Q as well as the baseflow decay function were chosen with the goal of identifying as many single peak events as possible (Figure S3).

For comparison, events were also defined by periods where daily Q exceeded baseflow ( $+20\%$ ). Baseflow was determined using the R package hydrostats (Bond, 2019), with alpha set to 0.925, and reflection to 30 based on Ladson et al. (2013).

## 2.2.2 | Event analysis

Identified events were subject to qualitative and quantitative analysis of their characteristics. For qualitative analysis, data was plotted and

visually inspected. Events were divided into three categories: (1) low (mean event Q  $0\text{--}2 \text{ m}^3/\text{s}$ ), (2) intermediate (mean event Q  $2\text{--}11 \text{ m}^3/\text{s}$ ) and (3) high (max Q  $15\text{--}45 \text{ m}^3/\text{s}$ ). Identification of the threshold between low and intermediate Q was based on a spectral density analysis in which a Fourier decomposition of Q was performed for each event where the intensity of frequencies was visualized in a periodogram and the results interpolated by smoothing (JMP, 2021). The breakpoint for high Q events was semi-qualitatively selected.

Events were quantitatively analysed with hysteresis indexes (HI) (Lloyd et al., 2016) to facilitate comparison despite different characteristics and properties. When possible, previously identified events were trimmed so that they had approximately the same start and end Q. The rising/falling section of the hydrograph was identified, Q and HF turbidity were normalized following Lloyd et al. (2016) (equations in Table S1). Normalized Q was sectioned into 10% increases/decreases (Figure 2), and normalized turbidity averaged for observations that fell within these windows. To calculate HI, falling limb turbidity (normalized and averaged per 10% Q increase/decrease) ( $FL_{Turb\_norm}$ ) was subtracted from rising limb turbidity ( $RL_{Turb\_norm}$ ) for each 10% increment ( $HI_{0.1}\text{--}HI_1$ ) (Figure 2). The resultant 10 values were then averaged across the whole event ( $HI_{mean}$ ). Lloyd et al. (2016) showed that calculating HI for every 10% increment of Q produces a robust result over different hysteresis sizes and shapes. The magnitude of HI reflects the magnitude of difference between rising and falling limbs, furthermore values close to zero typically indicate complex hysteresis patterns (Lloyd et al., 2016).

$$\text{Hysteresis index}_{0.1\text{--}1} = RL_{Turb\_norm} - FL_{Turb\_norm} \quad (1)$$

Hysteresis patterns were categorized into five different types (Figure 3) based on the calculated hysteresis indexes. Clockwise loops (C) indicate a fast response where readily available turbidity sources in close proximity to the stream are mobilized with the increasing flow but are then depleted during hydrograph recession (Haddadchi & Hicks, 2020b; Lloyd et al., 2016). Anticlockwise (A) loops are caused

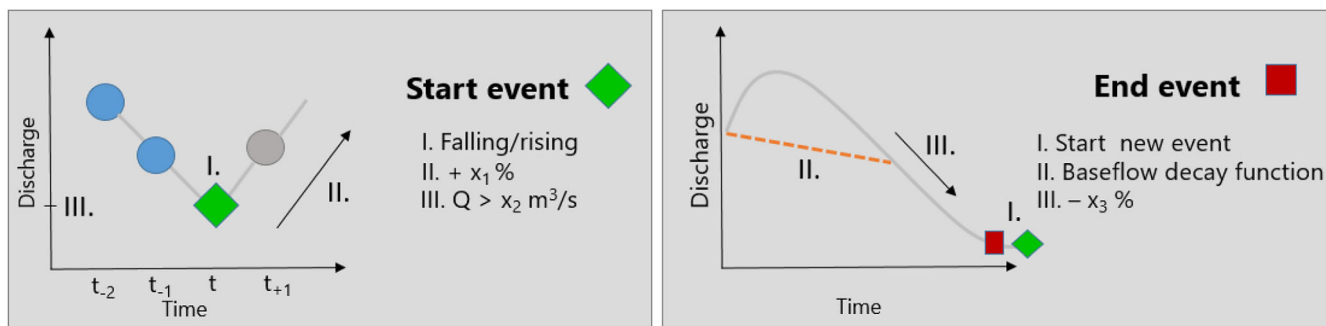
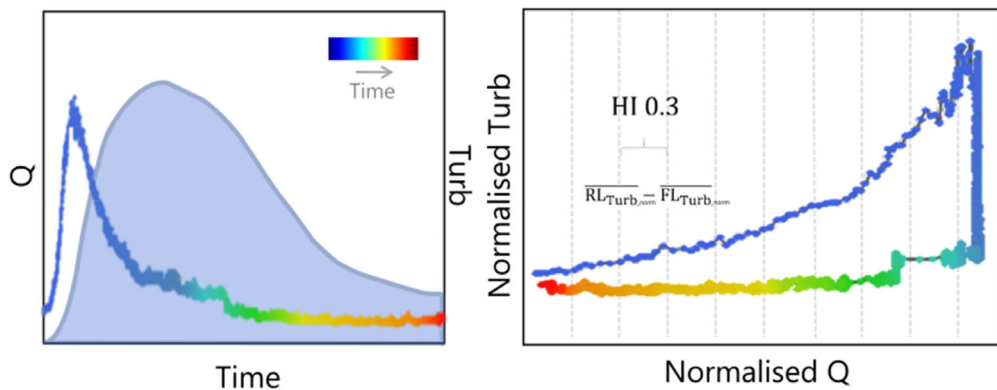


**FIGURE 1** Description of conditions for starting (I-III)/ending (I-III) an event, the start of an event (left panel) is indicated by the green diamond shape (t) and (I) needs to follow a specific pattern for observations on the rising/falling limb of the hydrograph, blue circles are discharge observations two time steps before the start of the event ( $t_{-1}, t_{-2}$ ) and grey circle one-time step after ( $t_{+1}$ ), (II)  $x_1$  denotes a percentage change in discharge between t and  $t_{+1}$  (e.g.,  $1.2\%$ ), (III)  $x_2$  denotes a Q threshold (e.g.,  $>0.1 \text{ m}^3/\text{s}$ ). The conditions to end an event (right panel) includes (I) the start of a new event (green diamond), (II) a baseflow decay function (indicated as the orange dotted line) and (III)  $x_3$  a percentage decrease between to following observations (e.g.,  $>0$ )

**FIGURE 2** Example of an event (left) and calculation of HI index with 10% increments (right), time indicated by colour



by a slower response of turbidity in relation to  $Q$  increase. This could indicate that material is transported from more distant sources (Haddadchi & Hicks, 2020b; Williams, 1989) or that an erosion event following soil saturation is the sediment source (Williams, 1989). More complex hysteresis patterns were also identified. Figure-eight patterns indicate that two or more turbidity sources are active. Figure-eight patterns with a clockwise loop for low  $Q$ , and anticlockwise for high  $Q$  (Clockwise-Anticlockwise-CAC) occur when readily available turbidity sources are mobilized early in the event until exhaustion of these sources following material arriving from more distant sources (Haddadchi & Hicks, 2020b). Figure-eight patterns with an anticlockwise pattern for low  $Q$  and clockwise for high  $Q$  (Anticlockwise-Clockwise-ACA) could occur when sources of turbidity are activated late in the flood recession. Complex patterns (with more than two linked hysteresis loops) are a result of several turbidity peaks in relation to the  $Q$  increase/decrease.

Hysteresis indexes were then matched with event characteristics (Table S2) and prevailing environmental conditions. Precipitation and temperature (10 min resolution) monitored 7 km (central Uppsala) from the sensor location was coupled to the events. Precipitation was summed over the event duration as well as for 2, 5 and 10 days before the event. Antecedent moisture estimated as soil moisture deficits (SMD), hydrologically effective rainfall (HER), precipitation falling as snow, snowmelt and snow depth were all modelled with the rainfall/runoff model PERSiST on a daily time step (Futter et al., 2014). The SMD is an estimate of the difference between soil water holding capacity and soil water content. An SMD of 0 is indicative of a saturated soil. Higher SMD values are indicative of a drier catchment where a greater fraction of incoming precipitation will contribute to catchment recharge and a smaller fraction to runoff. The HER is an estimate of the amount of rainfall or snowmelt contributing to runoff, hence it represents precipitation minus evaporation. Snowfall, snowmelt and snow depth (expressed as snow water equivalents) were all estimated in PERSiST using a degree-day melt model calibrated against observed  $Q$ .

The model was calibrated using a protocol described by Ledesma et al. (2012). An initial manual calibration was used as a starting point for a Monte Carlo exploration of parameter space using the method of Futter et al. (2014). The best performing parameter set from the Monte Carlo analysis was then subject to a final manual tuning to generate the model setup used here. Model performance was evaluated

against the Nash Sutcliffe statistic for untransformed data (NS), log-transformed data (logNS) and the ratio of variances in the observed and modelled time series. This last constraint was necessary as calibration only to NS or logNS tends to simulate lower variances in the modelled output than are seen in the observed data. The calibration was performed using observed streamflow data from 1 October 2011 to 31 December 2019. The forcing time series of daily temperature and precipitation were obtained from a monitoring station in central Uppsala (7 km from the sensor location).

Other descriptors used to characterize events included: season, storm event duration, time interval between two events; a suite of parameters describing change in  $Q$  (min/max/mean  $Q$ , mean  $Q$  24 h before the event, range in difference  $Q$  and % increase of  $Q$ ); and a suite of parameters describing change in turbidity (min/max/mean, range in turbidity difference and % increase of turbidity). The data set was explored using principal component analysis (PCA) in the software CANOCO 5 (ter Braak & Smilauer, 2012). Variables included in the final PCA were identified using a procedure documented by King and Jackson (1999). Due to the large number of possible descriptors (60, Table S3) a selection of the most influential variables to include in the PCA ordination was performed using method B2 in which variables are rejected backwards from the last component (King & Jackson, 1999). King and Jackson (1999) state that the ratio between observations to variables should be at least 3:1 to ensure stability and reliability of any multivariate analysis, therefore we retained the 20 most influential variables in the final ordination. The final ordination based on the 20 selected variables was compared to the original full ordination using a Procrustes analysis, which indicated only small differences between the two ordinations.

### 3 | RESULTS

#### 3.1 | Event identification

The event definition procedure both influences and constrains subsequent analysis of hysteresis patterns. Our method identified 117 unique events during the study period (2012–2019). The 76 events retained for further analysis had turbidity measurements for  $\geq 95\%$  of the event. Event duration varied between 5 and 80 days

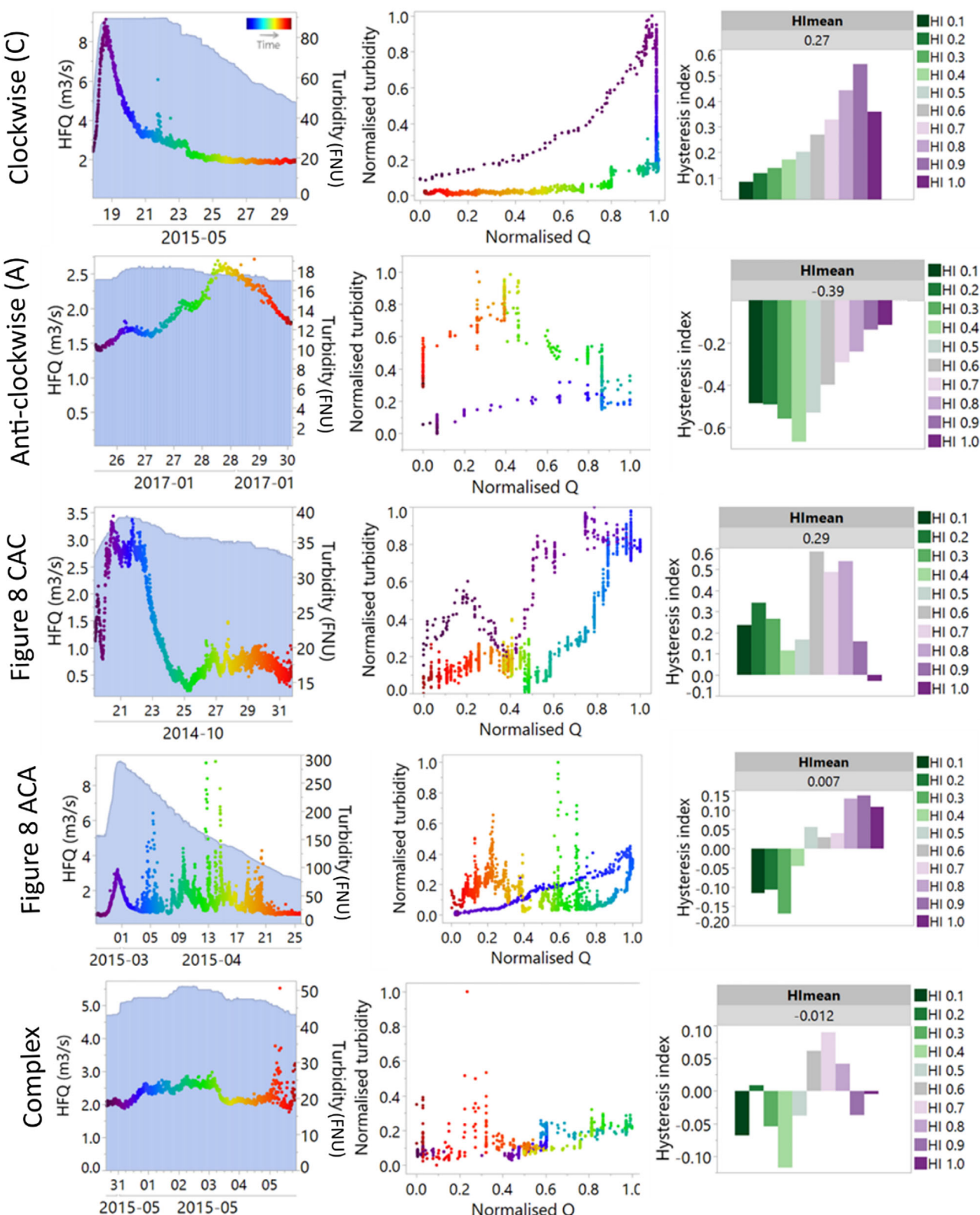


**FIGURE 3** The different kinds of hysteresis loops with the left panel describing Q (left y-axis) in relation to turbidity response (right y-axis) over time (x-axis), middle panel the hysteresis loop with normalized turbidity (y-axis) and normalized Q (x-axis). The right panel describes hysteresis indexes (HI) from 0.1–1 as well as  $HI_{mean}$  for the different event types

with an average of 17 days and covered a wide flow range (max Q between 0.2 and 45 m<sup>3</sup>/s, representing 99.6% of the monitored Q range). However, not all turbidity events were captured with the

event definition method used here (focusing on Q variation); some turbidity events occurred for example on the falling limb of the hydrograph (Figure 4, Table S4).

The event definition procedure presented here was compared to events defined using the R package hydrostats (Bond, 2019) which is commonly used for event definition in similar studies (e.g., Hashemi et al., 2020). Using hydrostats, 70 events were identified for the study period and 52 had turbidity data. Since this method was based on a 20% deviation from baseflow, the event duration was in general longer (Figure S3), ranging between 2 and 125 days with an average of 32 days. With the hydrostats event definition method it was, however, impossible to analyse hysteresis indexes in many events due to multiple Q peaks (Figure S3).

### 3.2 | Qualitative analysis of events

When visually inspecting the identified events, three different reoccurring patterns were identified (Figure 5). Events with low mean  $Q$  ( $<2 \text{ m}^3/\text{s}$ ) often showed short-term, quasi-periodic variation in turbidity, to a large extent disconnected from  $Q$  variation. Spectral density analysis indicated that all events with a mean event  $Q$  of below  $2 \text{ m}^3/\text{s}$  show periodic variation with frequencies between 8 h and 3 days (Figure S4). The maximum  $Q$  for events with this turbidity

pattern ranged from 0.2 to  $2.1 \text{ m}^3/\text{s}$  ( $n = 34$ ). The majority of these events occurred during summer ( $n = 17$ ), with some events in autumn ( $n = 8$ ), spring ( $n = 7$ ) and winter ( $n = 2$ ). Events lasted on average for 15 days. The mean turbidity during these events was 10 FNU, the median amplitude of turbidity variation was low (10 FNU), as was mean HFQ ( $1 \text{ m}^3/\text{s}$ ). The timing of the turbidity peaks could not be attributed to a specific time of the day and peaks also occurred during periods with no identified events (no large  $Q$  variations).

Four events with high maximum  $Q$  ( $>15 \text{ m}^3/\text{s}$ ) occurred during winter ( $n = 1$ ) and spring ( $n = 3$ ) and were between 29 and 54 days long. All events ( $n = 4$ ) were connected to the spring flood or large snowmelt events. Turbidity peaks were disconnected from  $Q$  variation. Mean turbidity during these events was 70 FNU, but ranged between 8 and 4955 FNU, mean HFQ was  $11.5 \text{ m}^3/\text{s}$  but ranged between 1.6 and  $45 \text{ m}^3/\text{s}$ .

Thirty-eight events were in the intermediate range of  $Q$  (mean  $Q > 2 \text{ m}^3/\text{s}$ , max  $Q < 15 \text{ m}^3/\text{s}$ ). These events often showed an early turbidity response, followed by a second peak after  $Q$  decreased. The events ( $n = 38$ ) were equally distributed between spring ( $n = 14$ ), autumn ( $n = 15$ ) and winter ( $n = 9$ ). Mean turbidity during these events were 27 FNU, ranging between 2 and 873 FNU, mean HFQ

**FIGURE 4** Turbidity events within and outside of hydrological events in the years of 2015–2016. Events are indicated by grey areas. The top panel is describing precipitation (mm) indicated by blue dots, the middle panel soil moisture deficit (mm) indicated by black line, and lower panel left axis HFQ ( $\text{m}^3/\text{s}$ ) indicated by blue shaded areas and lower panel right axis turbidity (FNU) indicated by black dots

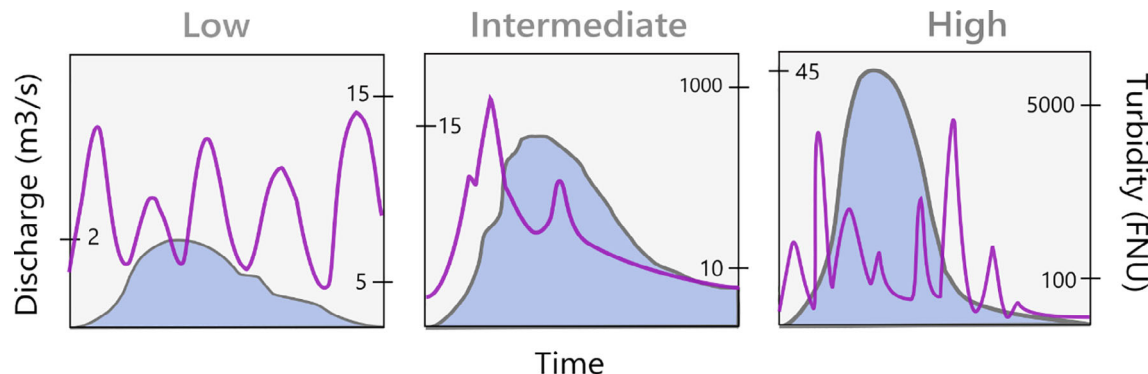
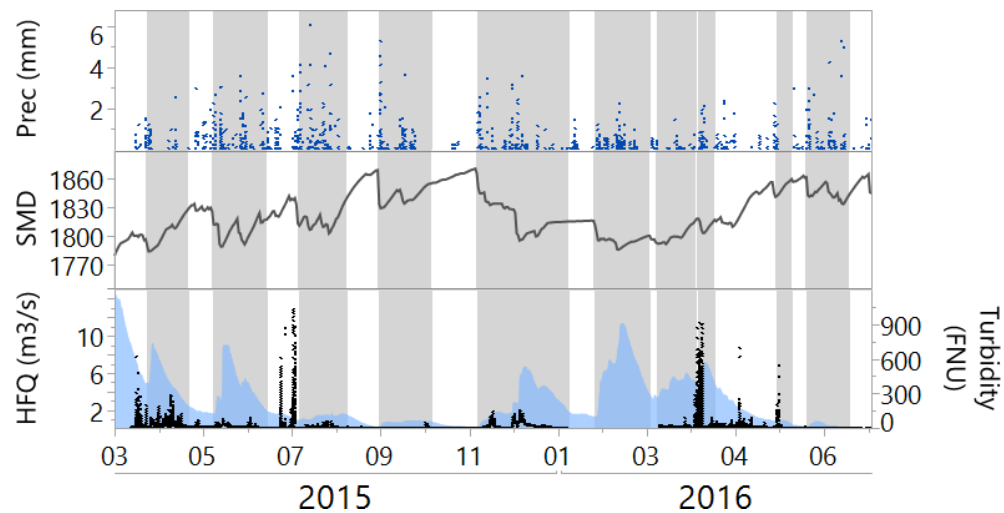


**FIGURE 5** A conceptual picture of different c-q responses during low, intermediate and high  $Q$ . blue area indicates  $Q$  and purple line turbidity. Note the differences in scale for  $Q$  and turbidity between the plots

**TABLE 1** Characteristics of the different groups of events defined by hysteresis index type

	H <sub>mean</sub>	P <sub>event</sub>	SMD	SF <sub>event</sub>	SM <sub>event</sub>	Q <sub>event</sub>	Duration	Interval events	Amp HFQ	Amp Turb	Season (Winter, Spring, Summer, Autumn)
<b>C (n = 23)</b>											
Min	0.04	0	42	0	0	1.7	3	0	0	3	
Max	0.48	61	101	98	137	15.5	50	206	43	4946	
Mean	0.30	17	68	15	23	-	16	34	4	338	
%	-	91	-	43	61	-	-	-	-	-	
<b>CAC (n = 7)</b>											
Min	0.03	0	55	0	0	0.1	2	5	0.1	5	
Max	0.30	16	126	58	17	11.2	15	71	4.3	538	
Mean	0.18	7	86	8	3	-	8	37	1.1	93	
%	-	71	-	14	29	-	-	-	-	-	
<b>A (n = 7)</b>											
Min	-0.39	0	68	0	0	0.8	4	0	0.1	4	
Max	-0.13	25	116	0	0	4.7	15	34	0.5	28	
Mean	-0.25	6	90	0	0	-	7	16	0.3	13	
%	-	57	-	-	-	-	-	-	-	-	
<b>ACA (n = 6)</b>											
Min	-0.20	2	50	0	0	0.3	3	1	0.0	3	
Max	0.17	16	118	39	31	9.7	19	118	4.5	273	
Mean	0.00	9	81	7	7	-	8	32	1.4	68	
%	-	100	-	33	33	-	-	-	-	-	
<b>Complex (n = 17)</b>											
Min	-0.17	0	46	0	0	0.2	2	0	0.1	2	
Max	0.44	55	117	76	17	6.5	24	251	1.0	80	
Mean	0.02	14	86	5	2	-	9	27	0.4	17	
%	-	94	-	18	29	-	-	-	-	-	

Note: Min max and mean, mean hysteresis index for the event ( $H_{mean}$ ), precipitation during the event ( $P_{event}$ , mm), mean soil moisture deficit during the event ( $P_{event}$ , mm), mean snowfall during the event ( $SM_{event}$ , mm), mean Q during the event ( $Q_{event}$ ,  $m^3/s$ ), duration of event, interval between events, change of Q during the event (amp Turb) and season. For each shape the share of events displaying, for example, precipitation, snowfall, snowmelt is presented in %.

was  $5 \text{ m}^3/\text{s}$ , ranging between  $0.19$  and  $14 \text{ m}^3/\text{s}$ . Events lasted on average for 15 days.

In the analysis of successive events, some events appeared to affect each other where the first event gave a large turbidity response compared with the following (Figure S5, e.g., ID 38–41, ID 42–46, ID 82–85, ID 103–104). However, this was not the case for all successive events.

### 3.3 | Quantitative analysis of events

During the studied years (2012–2019) a subset of 60 events (compared with the original 76) were identified and hysteresis indexes calculated. For these 60 events, it was possible to identify a clear start with increasing Q, and after the peak a return to approximately the same Q. Events were equally distributed between seasons (Table 1).

The events showed heterogeneous HI: 23 events showed a clockwise response, seven events an anticlockwise response, seven events a CAC response, six events an ACA response and 17 a complex response. Hysteresis indexes ( $\text{HI}_{\text{mean}}$ ) ranged between  $-0.39$  and  $0.48$ . Clockwise responses ranged between  $0.04$  and  $0.48$ , anticlockwise responses between  $-0.13$  and  $-0.39$ , CAC responses between  $0.03$  and  $0.30$ , ACA responses between  $-0.2$  and  $0.17$  and complex responses between  $-0.17$  and  $0.44$ . CAC events were often changing sign for  $\text{HI}_1$  (6/7 events) which indicates a loop only for the high Q (Figure 3).

Most events were connected to rainfall events, especially those with clockwise (91%), ACA (100%) and complex (94%) hysteresis patterns (Table 1). During 43% of the clockwise events there was snowfall, in 61% of the events snowmelt and the mean SMD was indicative of wetter conditions. Anticlockwise events were not connected to either snowfall or snowmelt, but in 57% of the events to rainfall.

Anticlockwise events showed small changes in both HFQ ( $0.3 \text{ m}^3/\text{s}$ ) and turbidity (13 FNU). A similar response was also seen for complex events (HFQ  $0.4 \text{ m}^3/\text{s}$ , turbidity 17 FNU). Event duration was generally longer for clockwise responses compared to anticlockwise, CAC, ACA and complex responses, while the interval between events was shorter for anticlockwise events (16 days).

Many summer events were connected to low Q, and showed a complex hysteresis pattern (Figure 6). The majority of autumn, spring and winter events gave a clockwise hysteresis response, while none of the summer events did. The anticlockwise responses were connected to lower mean Q ( $0.15$ – $6.5 \text{ m}^3/\text{s}$ ), while the clockwise responses occurred with higher mean Q ( $1.2$ – $15 \text{ m}^3/\text{s}$ ). Many of the ACA and CAC responses have only a few hysteresis indexes that are changing from positive to negative or vice versa, while the complex responses often have many indexes shifting around 0.

In the PCA (Figure 7) the first two axes explain 48% of the variation. According to King and Jackson (1999) parameter selection method, weather related parameters, seasons and hysteresis patterns were all important. Clockwise events were associated with winter and spring season and Q parameters, that is, maximum HFQ, maximum snowmelt (maxSM). The spring season was related to maximum snowmelt and HFQ, while the winter season was correlated to mean snow depth (meanSD), accumulated snowfall (accSF), Q 10 days before the event (Qd-10), accumulated hydrologically effective rainfall (accHERd-5) as well as minimum turbidity concentration during the events (minTurb). Maximum turbidity (maxTurb), event duration, falling limb duration (duration, durationFL), the amplitude of Q change (ampHFQ), accumulated precipitation (accPrec) and snowmelt (accSM) were correlated. Anticlockwise, ACA and CAC responses are connected to precipitation on the start day of the event (Precd0) as well as soil moisture deficit on the start day of the event (SMDd0). The summer season was associated with complex hysteresis patterns, mean soil

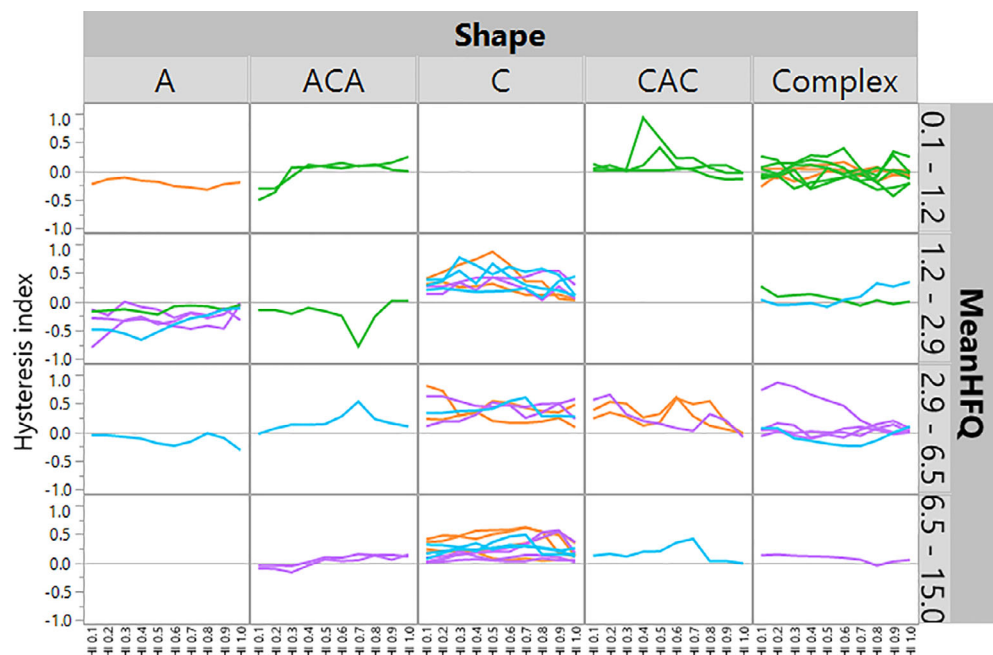


**FIGURE 6** Events divided by shape and mean HFQ showing the varying hysteresis indexes (HI) over the events, seasons are indicated by colour where; winter-blue, autumn-orange, summer-green, spring-purple,  $n = 60$

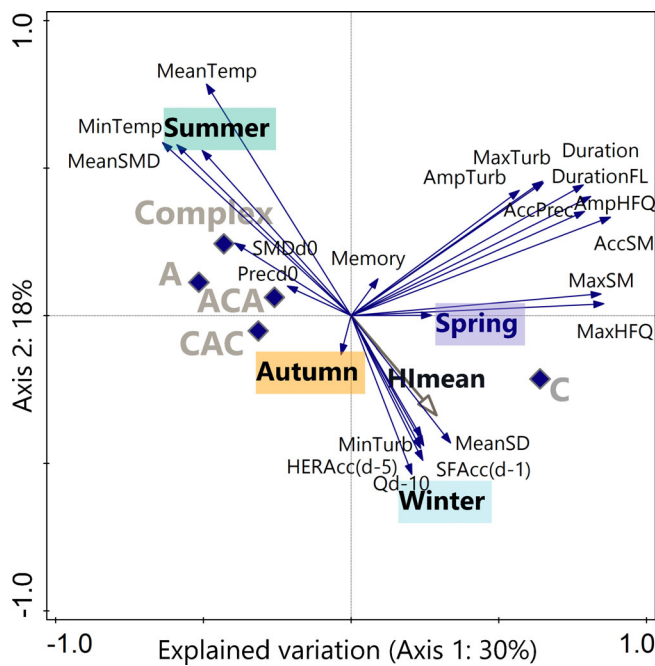


**FIGURE 7** Principal component analysis (PCA) of relevant environmental parameters and shapes of hysteresis loops. The PCA explains 48% of the total variation in two axis,  $n = 60$

moisture deficit (meanSMD) and mean temperature (meanTemp). Not all parameters were clearly connected to a hysteresis pattern.

## 4 | DISCUSSION

The study explores the potential for describing meso-scale catchment function based on hysteresis patterns extracted from HF turbidity-Q data. We corroborated our hypothesis that hysteresis patterns would vary depending on whether  $Q$  was low or high. Our analysis showed that change in turbidity was correlated to  $Q$  only between the 50th and 97.5th percentiles of the  $Q$  range. Turbidity variation within events was not strongly correlated to  $Q$  during low (mean  $Q < 2 \text{ m}^3/\text{s}$ ) and high (max  $Q > 15 \text{ m}^3/\text{s}$ ) flow periods. Turbidity events were also observed with no driving  $Q$  change. The different  $Q$  regimes had a strong effect on the HF turbidity-Q relationships but not the specific hysteresis patterns.

### 4.1 | The presence of a turbidity-Q relation

By analysing hysteresis patterns and using the hysteresis indexes of Lloyd et al. (2016) we could make some observations about catchment processes that partly corroborated our hypothesis that hysteresis patterns vary seasonally as clockwise hysteresis responses were connected to the wetter winter and spring seasons. The fast response of mobilized material in the stream associated with precipitation, snowfall or snowmelt was observed in around a third of the identified events (23/60). These events are probably source limited and the

material could be mobilized from the stream channel, adjacent riparian areas (Sherriff et al., 2016), during snowmelt (Malutta et al., 2020) or through tile drains (Bowes et al., 2005). Antecedent moisture conditions have previously been shown to be important for fast mobilization and clockwise hysteresis events (Bowes et al., 2005), as pre-wetted material can have faster erosion rates (Lawler et al., 2006). Clockwise events were associated with a lower mean SMD suggestive of wetter antecedent conditions compared to the other groups (Table 1), as well as appearing as a negative correlation in the PCA (Figure 7). Rose et al. (2018) observed mainly clockwise patterns in a stream where the transport consisted of mainly fines. Turbidity in Sävjaån has previously been hypothesized to be affected by colloidal material since a large proportion of the soil in the area close to the sensor consists of clay (Lannergård et al., 2019). Clockwise events are often associated with sources close to the monitoring station (Haddadchi & Hicks, 2020b; Lloyd et al., 2016), which means that the size of Sävjaån catchment might not be a factor that influences this response.

Generally, the change in  $Q$  and turbidity was small for the anti-clockwise hysteresis patterns observed in seven events, these events were not connected to snowfall or snowmelt but the PCA showed a correlation to precipitation on the start day of the event (Figure 7). Anticlockwise responses have been connected to travel time from distant sources or erosion events (Williams, 1989). In Sävjaån these events seem to be transport rather than source limited, based on the small differences in both  $Q$  and turbidity. Since the catchment is large and the travel time from the furthest part of the catchment was estimated at between 2 and 5 days, this could affect anticlockwise, ACA and CAC hysteresis shapes (transport of e.g., plankton or sediment).

Tananaev (2015) showed that frozen soil would give a negative hysteresis index effect (HI below 0) due to the need to develop an active soil layer before mobilization of material could occur. In this study anticlockwise events were not correlated to any of the winter season, snowfall or snowmelt, so this was not generally consistent in Sävjaån catchment. Perks et al. (2015) observed anticlockwise events for suspended sediment at low magnitude events, which they interpreted as delivery via artificial sub-surface pathways, for example, piping erosion. Normally, transport via tile drains is connected to a fast response (Bowes et al., 2005; Sherriff et al., 2016) but studies have also attributed contribution from tile drains to what we interpret as figure-eight patterns (ACA, CAC, Eder et al., 2010). This indicates that there could be a fast response combined with a temporal delay since the water is passing through the soil.

A figure-eight shape with a clockwise loop for low  $Q$  and anti-clockwise for high  $Q$  (CAC), could occur when readily available sources are exhausted with subsequent mobilization of material from more distant sources (Haddadchi & Hicks, 2020b). This could also depend on overlapping input from sources (Tananaev, 2015) or that hydrological connectivity increase during the event (Rose et al., 2018). The opposite pattern with an anticlockwise loop during low  $Q$  and clockwise high  $Q$  (ACA) could occur when proximal sources are activated late during the event (e.g., erosion, bank collapse) (Haddadchi & Hicks, 2020b). Due to the increased complexity of a meso-scale

catchment, these responses were expected to be frequent. Seven events were interpreted as CAC events and six as ACA events. In many (10/13) of the studied CAC and ACA events, one or several of the turbidity peaks was associated with precipitation (Figure S6). All ACA events were connected to precipitation during the event. ACA and CAC events indicate supply limitation from two or more sources of material mobilized and contributing to turbidity with different travel times for example, from different parts of the catchment. It could also be connected to hydrological connectivity, where different areas are connected to the stream depending on, for example, wetness of the soil. However, it is clear that many different processes result in the same hysteresis category (e.g., A, ACA, CAC) which makes it a simplification to assign one process per hysteresis pattern. The theoretical categorisation is not able to separate the processes of the system fully, thus results must be interpreted with caution. To further explore the different patterns and sources of material production and delivery, several turbidity sensors and water-level loggers could be deployed in the catchment (e.g., in forested areas, downstream the lakes, in critical source areas for erosion).

Complex hysteresis patterns were identified for 17/60 studied events, these often occurred during summer and low Q. In the PCA, the summer season was correlated to mean SMD and mean precipitation during events, indicative of generally drier conditions and precipitation driven events. However, in this study low Q events were in most cases associated with short time variation (see coming section) where turbidity and Q were uncoupled. Complex hysteresis patterns have previously been connected to heterogeneous spatial and temporal distribution of rainfall events (Haddadchi & Hicks, 2020b).

When analysing successive events, turbidity sources were in some cases depleted, indicating source limitation. Source limitation where the previous event controls material availability in the subsequent event have previously been shown (Bowes et al., 2005; Haddadchi & Hicks, 2020b; Jordan et al., 2005). Bowes et al. (2005) observed a change in sign of the hysteresis index where early events in the succession gave a clockwise response and later ones an anti-clockwise response. This could, however, not be confirmed in this study possibly due to the larger scale of the catchment where several sources could contribute to transport over time.

Our third hypothesis was that event characteristics (e.g., duration) would affect hysteresis patterns. The most important variables included in the PCA analysis were maximum Q (MaxHFQ), duration of the falling limb (DurationFL) and minimum turbidity (MinTurb). Many explanatory variables were excluded from the plot, for example, minimum and mean HFQ. A full list of explanatory variables that did and did not fulfil the selection criteria are presented in Table S5. In previous studies variable rainfall intensities, antecedent soil water content, total runoff amounts (Eder et al., 2010), flood event total runoff, flood duration (Haddadchi & Hicks, 2020b) have been identified as most relevant for the hysteresis direction. In this study precipitation on the first day of the event as well as accumulated precipitation during the event were relevant, along with mean SMD during the event, different Q characteristics and event duration.

## 4.2 | Absence of a turbidity-Q relation

### 4.2.1 | Short term variation

Short time turbidity variation was observed for all low Q events, with a period ranging between 8 h and 3 days (example in Figure S4). Hysteresis index analysis are sensitive to diel cycles (Heathwaite & Bieroza, 2020), and the assumption of a connection between turbidity and Q is not fulfilled for these events. The events showed a general low turbidity (average 10 FNU) and amplitude of turbidity variation (10 FNU), as well as a low mean Q ( $<1\text{ m}^3/\text{s}$ ). The timing of the turbidity peaks could not be attributed to a specific time of the day and peaks also occurred during periods with no identified flow events (no large Q variations). It is hard to find a common explanation for the short term turbidity variation in Sävjaån. Short term variations in turbidity have previously been explained as a result of biological factors including bioturbation (Loperfido et al., 2010), invertebrate activity (grazing/drift), fish feeding, or primary production (Gillain, 2005). However, in these cases the cycles have been connected to the time of the day, which could not be shown in this study. The low Q events also occurs during all seasons, which makes it unlikely that the origin of the variation is biological.

The variation could also be caused by anthropogenic influence, for example from running an irrigation pump but also here it would be unlikely that water would be needed for irrigation outside the growing season between November and March (5 events). Since the variation exists also when there are no events, they are also not necessarily connected to processes derived from Q variation. Further studies are needed to explore this variation, especially since high concentrations, for example, TP during summer low flow could have a large impact in the river causing excessive plant/algae growth and oxygen deficiency (Jarvie et al., 2005). It is however important to note that for many of the events both the mean turbidity and amplitude of turbidity variation are low (10 FNU, 10 FNU). To explore these variations further could give a deepened ecological understanding as well as understanding of active processes that are influencing the turbidity in the stream.

### 4.2.2 | Spring flood and snowmelt

Events above the 97.5th percentile of the Q range also showed a disconnection between turbidity and Q hysteresis. These events were connected to the yearly spring flood or snowmelt. In these cases, hydrological connectivity is likely very high and multiple processes (e.g., snowmelt from different parts of the catchment, erosion and gradual melting of frozen soil) that increase turbidity in the stream occur simultaneously. It is therefore hard to interpret the turbidity in relation to Q. These events are nevertheless critical for managers, since they could potentially transport substantial loads (of, e.g., TSS and TP) to surface waters and the Baltic Sea.

#### 4.2.3 | Turbidity events

When turbidity events were observed without any variation in Q, they often occurred on the falling limb of the hydrograph (5/7 events) (Table S4). In 5/7 events the turbidity peaks were connected to precipitation the same day or within the three previous days without a response in the hydrograph, and in 5/7 cases soil moisture deficit was increasing. In a study by Jordan et al. (2005), non-storm P transfers were considered important, and the hypothesis was that they came from rural point sources and consisted mostly of particulate P. In this study, we can conclude that there are significant turbidity events occurring at certain times, and it raises the question if we could use high-resolution turbidity monitoring to define events, instead of or in combination with Q variation. Concentration events could then show importance of processes regarding stream ecology, while events defined by Q are more important for transport of material. To continue analysing the turbidity-TP and TSS relationship in the intermediate Q range could give further insight into important processes operating in the catchment.

#### 4.3 | Management implications

As the catchment area increases, more physical processes, heterogeneous environmental conditions and site specific characteristics (land use, soil type) (Gao & Josefson, 2012) are integrated into the stream water quality signal we are trying to interpret. Despite the size of Sävjaån catchment ( $722 \text{ km}^2$ ), the study showed that insights about what processes might be delivering material downstream could help to point out especially important mitigation measures. The fast clockwise pattern indicating a local source of turbidity, for example, stream bed, bankside erosion or fast flushing through tile drains. This observed pattern shows the importance of working with near-stream measures (compared with e.g., field measures). Our results highlight the importance of (1) riparian vegetation preferably during large parts of the year (during winter and snowmelt these areas have no ground cover in Sävjaån) to decrease mobilization of particles in the near stream area, (2) use of buffer strips/set-aside areas (Verstraeten et al., 2006), (3) drain discharge on vegetated areas, and (4) cover crops (Aryal et al., 2018).

Overland flow as a potential contributor of turbidity can be limited by, for example, structure liming (Aronsson et al., 2019) and efficient tile drainage (Golmohammadi et al., 2017). Structure liming of clay soils, is a measure that improves soil stability, porosity and aggregate strength, thus reducing losses of particulate P (Ulén & Etana, 2014). By improving the soil structure, drainage losses of particles is minimized. Wenng et al. (2021) have shown that little vegetation cover and high intensity of soil tillage led to high hysteresis indexes, indicating large amounts of transported material.

The transport limited anticlockwise events are less management relevant due to the low magnitude of Q and turbidity change. More insights could be developed regarding the ACA and CAC events (with two or more sources to increase in turbidity) if we would increase our

spatial coverage and monitor several sites in the catchment or analyse a longer time period giving a larger number of sampled events. When precipitation causes a direct turbidity response in the stream vegetation in the riparian areas and buffer strips could counteract this mobilization of material. Regarding complex events and turbidity increases without Q variation we need to learn more about the underlying causes to formulate appropriate mitigation measures, this can be done by “adaptive” monitoring where grab samples are taken more frequently during these events/non-events.

Still, many different processes can give the same response (Bol et al., 2018; Lloyd et al., 2016), especially in larger catchments which makes it difficult to formulate specific catchment management plans based on the results presented here. From a management perspective it would be beneficial to identify which period that are important for transport of material, which periods that are important for the ecological status in the stream as well as which periods that are not so important. Analysis of hysteresis patterns for more than one parameter may also be a tool to deepen the understanding of prevailing processes in the catchment.

Many studies use HF turbidity as a proxy for suspended sediment and/or TP in studies analysis hysteresis relationships between turbidity and Q (Sherriff et al., 2016; Wymore, 2019; Ziegler et al., 2014). However, this assumes a linear relationship between the parameters, independent of rising/falling limb of the hydrograph (shown to be of importance by Stutter et al., 2017), seasonal changes in particle composition (Gippel, 1995) as well as particle size distribution possibly varying during an event (Pfannkuche & Schmidt, 2003; Walling & Moorehead, 1987). In the Sävjaån catchment, a good linear transfer function has been shown between turbidity and TP and TSS ( $r^2 = 0.64$ ,  $r^2 = 0.68$  for the years 2012–2017) (Lannergård et al., 2019). However, high levels of reactive P (PO<sub>4</sub>-P), colloids and influence of organic matter remains factors that might influence the relationship between turbidity versus TP and TSS and turbidity. Therefore, turbidity was not used as a proxy in this study since a deeper understanding is needed regarding the suitability of the relationships over different circumstances, especially when the aim of this study was to evaluate the suitability to identify processes transporting material in the catchment.

#### 5 | CONCLUSIONS

Efficient and informative data analysis of HF data are needed for the use of in-situ sensors in, for example, in national monitoring programmes. To gain insight into catchment function the HF turbidity-Q relationship was analysed, with data from a long term time series (2012–2019) representing all seasons, in a meso-scale northern mixed land use catchment.

Firstly, the study showed that the event definition method is the basis for assessing hysteresis patterns. Therefore, it is necessary to report how events are defined in studies using these indexes.

Second, a turbidity-Q relation was not apparent at all flows, but intermediate Q events (50th to 97.5th percentile of the Q range)

showed a connection between turbidity and Q within the events. Turbidity variation within events was not strongly correlated to Q during low (mean  $Q \leq 2 \text{ m}^3/\text{s}$ ) and high (max  $Q \geq 15 \text{ m}^3/\text{s}$ ) flow periods. Hence, the different Q regimes had a strong effect on the HF turbidity-Q relationships but not the specific hysteresis patterns; this falsifies the first part of the hypothesis.

Third, clockwise hysteresis patterns were often associated with precipitation, snowfall, snowmelt and wetter soils. The fast mobilization of material during these events could be counteracted by working with near-stream measures (e.g., riparian vegetation and buffer strips). Anticlockwise, ACA and CAC events could not be attributed to specific processes in the catchment, possibly due to the meso-scale of the catchment. Events also showed complex hysteresis patterns, often connected to the summer season and low Q displaying short time variation. Hence, the hysteresis shapes connected to seasons and event characteristics was confirmed, for example, clockwise and complex shapes but not all.

Turbidity events that were not associated with Q variation were observed, often on the falling limb of the hydrograph and connected to precipitation events that did not generate runoff. This indicates that we also have processes in the catchment causing mobilization of material that are not connected to Q variation, for example, precipitation on already wet riparian areas. By defining events based on actual increases in turbidity concentration and pairing the events with additional parameters as Q, precipitation, wetness indexes and other environmental conditions a deeper understanding of HF data could possibly be achieved.

Finally, analysis of HF turbidity-Q gave meaningful insight into catchment function, but these insights were not solely dependent on the analysis of hysteresis patterns. The use of qualitative and quantitative analysis methods investigating C-Q dynamics contributed to insights into turbidity generating processes over different flow ranges and seasons as a platform for some management relevant insights, such as limiting riparian connectivity to target the fast mobilization of material generated by an event.

## ACKNOWLEDGEMENTS

This study was funded by FORMAS (grant numbers: 2015-1518 and 2017-00029) and the Life-IP Rich Water Project. Special thanks to Majvor Nygren, Anton Berg and Emma Forslund who gave us permission to use the sensor location. A special thanks to Jelena Rakovic, Sara Sandström and Niklas Strömbäck for fruitful discussions.

## DATA AVAILABILITY STATEMENT

Data sets for this research are available at Figshare (10.6084/m9.figshare.14784738), as well as described in this paper and its supplementary information.

## ORCID

Emma E. Lannerård  <https://orcid.org/0000-0003-0301-1314>  
 Jens Fölster  <https://orcid.org/0000-0002-3069-4272>  
 Martyn N. Futter  <https://orcid.org/0000-0002-9789-7138>

## REFERENCES

- Aronsson, H., Berglund, K., Djodjic, F., Etana, A., & Geranmayeh, P. (2019). *Effekter av åtgärder mot fosforförluster från jordbruksmark och åtgärdsutrymme*. *Ekohydrologi* 160. SLU.
- Aryal, N., Reba, M. L., Straitt, N., Teague, T. G., Bouldin, J., & Dabney, S. (2018). Impact of cover crop and season on nutrients and sediment in runoff water measured at the edge of fields in the Mississippi Delta of Arkansas. *Journal of Soil and Water Conservation*, 73(1), 24–34. <https://doi.org/10.2489/jswc.73.1.24>
- Belmont, P., Gran, K. B., Schottler, S. P., Wilcock, P. R., Day, S. S., Jennings, C., Lauer, J. W., Viparelli, E., Willenbring, J. K., Engstrom, D. R., & Parker, G. (2011). Large shift in source of fine sediment in the upper Mississippi River. *Environmental Science & Technology*, 45(20), 8804–8810. <https://doi.org/10.1021/es2019109>
- Bieroza, M. Z., & Heathwaite, A. L. (2015). Seasonal variation in phosphorus concentration–discharge hysteresis inferred from high-frequency in situ monitoring. *Journal of Hydrology*, 524, 333–347. <https://doi.org/10.1016/j.jhydrol.2015.02.036>
- Bilotta, G. S., & Brazier, R. E. (2008). Understanding the influence of suspended solids on water quality and aquatic biota. *Water Research*, 42(12), 2849–2861. <https://doi.org/10.1016/j.watres.2008.03.018>
- Blann, K. L., Anderson, J. L., Sands, G. R., & Vondracek, B. (2009). Effects of agricultural drainage on aquatic ecosystems: A review. *Critical Reviews in Environmental Science and Technology*, 39(11), 909–1001. <https://doi.org/10.1080/10643380801977966>
- Bol, R., Gruau, G., Mellander, P.-E., Dupas, R., Bechmann, M., Skarbøvik, E., Bieroza, M., Djodjic, F., Glendell, M., Jordan, P., Van der Grift, B., Rode, M., Smolders, E., Verbeeck, M., Gu, S., Klumpp, E., Pohle, I., Fresne, M., & Gascuel-Odoux, C. (2018). Challenges of reducing phosphorus based water eutrophication in the agricultural landscapes of Northwest Europe. *Frontiers in Marine Science*, 5, 276. <https://doi.org/10.3389/fmars.2018.00276>
- Bond, N. *Hydrostats: Hydrologic Indices for Daily Time Series Data*. R package version 0.2.7. (2019). Available from <https://cran.r-project.org/web/packages/hydrostats/hydrostats.pdf>.
- Bowes, M. J., House, W. A., Hodgkinson, R. A., & Leach, D. V. (2005). Phosphorus–discharge hysteresis during storm events along a river catchment: The river swale, UK. *Water Research*, 39, 751–762. <https://doi.org/10.1016/j.watres.2004.11.027>
- Butturini, A., Alvarez, M., Bernal, S., Vazquez, E., & Sabater, F. (2008). Diversity and temporal sequences of forms of DOC and NO<sub>3</sub> -discharge responses in an intermittent stream: Predictable or random succession? *Journal of Geophysical Research*, 113(G3), G03016. <https://doi.org/10.1029/2008JG000721>
- Cassidy, R., & Jordan, P. (2011). Limitations of instantaneous water quality sampling in surface-water catchments: Comparison with near-continuous phosphorus time-series data. *Journal of Hydrology*, 405, 182–193. <https://doi.org/10.1016/j.jhydrol.2011.05.020>
- Coynel, A., Schafer, J., Hurtrez, J.-E., Dumas, J., Etcheber, H., & Blanc, G. (2004). Sampling frequency and accuracy of SPM flux estimates in two contrasted drainage basins. *Science of the Total Environment*, 330, 233–247. <https://doi.org/10.1016/j.scitotenv.2004.04.003>
- Defew, L. H., May, L., & Heal, K. V. (2013). Uncertainties in estimated phosphorus loads as a function of different sampling frequencies and common calculation methods. *Marine and Freshwater Research*, 64, 373–386. <https://doi.org/10.1071/MF12097>
- Djodjic, F. (2001). *Displacement of Phosphorus in Structured Soils*. [Doctoral thesis], Swedish University of Agricultural Sciences, Uppsala
- Eder, A., Strauss, P., Krueger, T., & Quinton, J. N. (2010). Comparative calculation of suspended sediment loads with respect to hysteresis effects (in the Petzenkirchen catchment, Austria). *Journal of Hydrology*, 389(1), 168–176. <https://doi.org/10.1016/j.jhydrol.2010.05.043>
- Evans, C., & Davies, T. D. (1998). Causes of concentration/discharge hysteresis and its potential as a tool for analysis of episode

- hydrochemistry. *Hydrogeochemistry and Water Chemistry*, 34(1), 129–137. <https://doi.org/10.1029/97WR01881>
- Fölster, J., Johnson, R. K., Futter, M. N., & Wilander, A. (2014). The Swedish monitoring of surface waters: 50 years of adaptive monitoring. *Ambio*, 43(1), 3–18. <https://doi.org/10.1007/s13280-014-0558-z>
- Fovet, O., Humbert, G., Dupas, R., Gascuel-Odoux, C., Gruau, G., Jaffrezic, A., Thelusma, G., Faucheux, M., Gilliet, N., Hamon, Y., & Grimaldi, C. (2018). Seasonal variability of stream water quality response to storm events captured using high-frequency and multi-parameter data. *Journal of Hydrology*, 559, 282–293. <https://doi.org/10.1016/j.jhydrol.2018.02.040>
- Futter, M. N., Erlandsson, M. A., Butterfield, D., Whitehead, P. G., Oni, S. K., & Wade, A. J. (2014). PERSIST: A flexible rainfall-runoff modelling toolkit for use with the INCA family of models. *Hydrology and Earth System Sciences*, 18(2), 855–873. <https://doi.org/10.5194/hess-18-855-2014>
- Gao, P., & Josefson, M. (2012). Event-based suspended sediment dynamics in a Central New York watershed. *Geomorphology*, 139–140, 425–437. <https://doi.org/10.1016/j.geomorph.2011.11.007>
- Gillain, S. (2005). Diel turbidity fluctuations in streams in Gwinnett County. *Proceedings of the 2005 Georgia Water Resources Conference*, held April 25–27, 2005, at the University of Georgia.
- Gippel, C. J. (1995). Potential of turbidity monitoring for measuring the transport of suspended solids in streams. *Hydrological Processes*, 9(1), 83–97.
- Glover, B. J., & Johnson, P. (1974). Variations in the natural chemical concentration of river water during flood flows, and the lag effect. *Journal of Hydrology*, 22, 303–316.
- Golmohammadi, G., Rudra, R., Prasher, S., Madani, A., Youssef, M., Goel, P., & Mohammadi, K. (2017). Impact of tile drainage on water budget and spatial distribution of sediment generating areas in an agricultural watershed. *Agricultural Water Management*, 184, 124–134. <https://doi.org/10.1016/j.agwat.2017.02.001>
- Gramlich, A., Stoll, S., Stamm, C., Walter, T., & Prasuhn, V. (2018). Effects of artificial land drainage on hydrology, nutrient and pesticide fluxes from agricultural fields – A review. *Agriculture, Ecosystems and Environment*, 266, 84–99. <https://doi.org/10.1016/j.agee.2018.04.005>
- Grayson, R. B., Finlayson, B. L., Gippel, C. J., & Hart, B. T. (1996). The potential of field turbidity measurements for the computation of total phosphorus and suspended solids loads. *Journal of Environmental Management*, 47(3), 257–267. <https://doi.org/10.1006/jema.1996.0051>
- Haddadchi, A., & Hicks, M. (2020a). Understanding the effect of catchment characteristics on suspended sediment dynamics during flood events. *Hydrological Processes*, 34(7), 1558–1574. <https://doi.org/10.1002/hyp.13682>
- Haddadchi, A., & Hicks, M. (2020b). Interpreting event-based suspended sediment concentration and flow hysteresis patterns. *Journal of Soils and Sediments*, 21, 592–612. <https://doi.org/10.1007/s11368-020-02777-y>
- Hansson, K., Ejhed, H., Widén-Nilsson, E., Johnsson, H., Tengdelius Brunell, J., Gustavsson, H., Hytteborn, J., Åkerblom, S. (2019) Näringsbelastningen på Östersjön och Västerhavet 2017, Sveriges underlag till HELCOM:s sjunde Pollution Load Compilation, Havs- och vattenmyndigheten rapport 2019:20
- Hashemi, F., Pohle, I., Pullens, J. W. M., Tornbjerg, H., Kyllmar, K., Marttila, H., Lepistö, A., Kløve, B., Futter, M., & Kronvang, B. (2020). Conceptual mini-catchment typologies for testing dominant controls of nutrient dynamics in three Nordic countries. *Water*, 12(6), 1776. <https://doi.org/10.3390/w12061776>
- Heathwaite, A. L., & Bieroza, M. (2020). Fingerprinting hydrological and biogeochemical drivers of freshwater quality. *Hydrological Processes*, 35, 1–17. <https://doi.org/10.1002/hyp.13973>
- Jarvie, H. P., Jürgens, M. D., Williams, R. J., Neal, C., Davies, J. J. L., Barrett, C., & White, J. (2005). Role of river bed sediments as sources and sinks of phosphorus across two major eutrophic UK river basins: The Hampshire Avon and Herefordshire Wye. *Journal of Hydrology*, 304(1–4), 51–74. <https://doi.org/10.1016/j.jhydrol.2004.10.002>
- JMP. (2021) Statistical Details for Spectral Density Available from <https://www.jmp.com/support/help/en/15.2/index.shtml#page/jmp/statistical-details-for-spectral-density.shtml>
- Johnes, P. J. (2007). Uncertainties in annual riverine phosphorus load estimation: Impact of load estimation methodology, sampling frequency, baseflow index and catchment population density. *Journal of Hydrology*, 332(1–2), 241–258. <https://doi.org/10.1016/j.jhydrol.2006.07.006>
- Jones, A. S., Horsburgh, J. S., Mesner, N. O., Ryel, R. J., & Stevens, D. K. (2012). Influence of sampling frequency on estimation of annual total phosphorus and total suspended solids loads. *Journal of the American Water Resources Association*, 48(6), 1258–1275. <https://doi.org/10.1111/j.1752-1688.2012.00684.x>
- Jordan, P., Arnscheidt, A., McGrogan, H., & McCormick, S. (2007). Characterising phosphorus transfers in rural catchments using a continuous bank-side analyser. *Hydrology and Earth System Sciences*, 11, 372–381. <https://doi.org/10.5194/hess-11-372-2007>
- Jordan, P., Arnscheidt, J., McGrogan, H., & McCormick, S. (2005). High-resolution phosphorus transfers at the catchment scale: The hidden importance of non-storm transfers. *Hydrology and Earth System Sciences*, 11, 685–691. <https://doi.org/10.5194/hess-9-685-2005>
- King, J. R., & Jackson, D. A. (1999). Variable selection in large environmental data sets using principal components analysis. *Environmetrics*, 10, 67–77. [https://doi.org/10.1002/\(SICI\)1099-095X\(199901/02\)10:1<67::AID-ENV336>3.0.CO;2-0](https://doi.org/10.1002/(SICI)1099-095X(199901/02)10:1<67::AID-ENV336>3.0.CO;2-0)
- Kirchner, J. W., Feng, X., Neal, C., & Robson, A. J. (2004). The fine structure of water-quality dynamics: The (high-frequency) wave of the future. *Hydrological Processes*, 18(7), 1353–1359. <https://doi.org/10.1002/hyp.5537>
- Knapp, J. L. A., von Freyberg, J., Studer, B., Kiewiet, L., & Kirchner, J. W. (2020). Concentration–discharge relationships vary among hydrological events, reflecting differences in event characteristics. *Hydrology and Earth System Sciences*, 24(5), 2561–2576. <https://doi.org/10.5194/hess-24-2561-2020>
- Kronvang, B., & Bruhn, A. J. (1996). Choice of sampling strategy and estimation method for calculating nitrogen and phosphorus transport in small lowland streams. *Hydrological Processes*, 10, 1483–1501. doi: 10.1002/(SICI)1099-1085(199611)10:11<1483::AID-HYP386>3.0.CO;2-Y
- Kronvang, B., Laubel, A., & Grant, R. (1999). Suspended sediment and particulate phosphorus transport and delivery pathways in an arable catchment, Gelbaek stream, Denmark. *Hydrological Processes*, 11(6), 627–642. doi:10.1002/(SICI)1099-1085(199705)11:6<627::AID-HYP481>3.0.CO;2-E
- Kuglerová, L., Hasselquist, E. M., Richardson, J. S., Sponseller, R. A., Kreutzweiser, D. P., & Laudon, H. (2017). Management perspectives on aqua incognita: Connectivity and cumulative effects of small natural and artificial streams in boreal forests. *Hydrological Processes*, 31(23), 4238–4244.
- Ladson, A. R., Brown, R., Neal, B., & Nathan, R. (2013). A standard approach to Baseflow separation using the Lyne and Hollick filter. *Australasian Journal of Water Resources*, 17(1), 25–34. <https://doi.org/10.7158/13241583.2013.11465417>
- Lana-Renault, N., Alvera, B., & García-Ruiz, J. M. (2011). Runoff and sediment transport during the snowmelt period in a mediterranean high-mountain catchment. *Arctic, Antarctic, and Alpine Research*, 43(2), 213–222.
- Langlois, J. L., Johnson, D. W., & Mehuijs, G. R. (2005). Suspended sediment dynamics associated with snowmelt runoff in a small mountain stream of Lake Tahoe (Nevada). *Hydrological Processes*, 19(18), 3569–3580. <https://doi.org/10.1002/hyp.5844>
- Lannergård, E. E., Agstam-Norlin, O., Huser, B. J., Sandström, S., Rakovic, J., & Futter, M. N. (2020). New insights into legacy

- phosphorus from fractionation of streambed sediment. *Journal of Geophysical Research*, 125(9), e2020JG005763. <https://doi.org/10.1029/2020JG005763>
- Lannergård, E. E., Ledesma, J. L. J., Fölster, J., & Futter, M. N. (2019). An evaluation of high frequency turbidity as a proxy for riverine total phosphorus concentrations. *Science of the Total Environment*, 651, 103–113. <https://doi.org/10.1016/j.scitotenv.2018.09.127>
- Lawler, D. M., Petts, G. E., Foster, I. D. L., & Harper, S. (2006). Turbidity dynamics during spring storm events in an urban headwater river system: The upper tame, west midlands, UK. *Science of the Total Environment*, 360(1–3), 109–126. <https://doi.org/10.1016/j.scitotenv.2005.08.032>
- Ledesma, J. L. J., Futter, M. N., Blackburn, M., Lidman, F., Grabs, T., Sponseller, R. A., Laudon, H., Bishop, K. H., & Köhler, S. J. (2018). Towards an improved conceptualization of riparian zones in boreal forest headwaters. *Ecosystems*, 21(2), 297–315. <https://doi.org/10.1007/s10021-017-0149-5>
- Ledesma, J. L. J., Köhler, S. J., & Futter, M. N. (2012). Long-term dynamics of dissolved organic carbon: Implications for drinking water supply. *Science of the Total Environment*, 432, 1–11. <https://doi.org/10.1016/j.scitotenv.2012.05.071>
- Lloyd, C. E. M., Freer, J. E., Johnes, P. J., & Collins, A. L. (2016). Technical note: Testing an improved index for analysing storm discharge-concentration hysteresis. *Hydrology and Earth System Sciences*, 20(2), 625–632. <https://doi.org/10.5194/hess-20-625-2016>
- Loperfido, J. V., Just, C. L., Papanicolaou, A. N., & Schnoor, J. L. (2010). In situ sensing to understand diel turbidity cycles, suspended solids, and nutrient transport in clear creek. *Water Resources Research*, 46(6), W06525. <https://doi.org/10.1029/2009WR008293>
- Malutta, S., Kobiyama, M., Chaffe, P. L. B., & Bonumá, N. B. (2020). Hysteresis analysis to quantify and qualify the sediment dynamics: State of the art. *Water Science and Technology*, 81(12), 2471–2487. <https://doi.org/10.2166/wst.2020.279>
- Möller, H. (1993). *Beskrivning till jordartskartan Uppsala NV =: Description to the quaternary map Uppsala NV*. Sveriges Geologiska Undersökning.
- National Land Survey. (2021) *Min Karta* Available from <https://minkarta.lantmateriet.se/>
- Outram, F. N., Lloyd, C. E. M., Jonczyk, J., Benskin, C. M. H., Grant, F., Perks, M. T., Deasy, C., Burke, S. P., Collins, A. L., Freer, J., Haygarth, P. M., Hiscock, K. M., Johnes, P. J., & Lovett, A. L. (2014). High-frequency monitoring of nitrogen and phosphorus response in three rural catchments to the end of the 2011–2012 drought in England. *Hydrology and Earth System Sciences*, 20, 3429–3448. <https://doi.org/10.5194/hess-18-3429-2014>
- Perks, M. T., Owen, G. J., Benskin, C. M. H., Jonczyk, J., Deasy, C., Burke, S., Reaney, S. M., & Haygarth, P. M. (2015). Dominant mechanisms for the delivery of fine sediment and phosphorus to fluvial networks draining grassland dominated headwater catchments. *Science of the Total Environment*, 523, 178–190. <https://doi.org/10.1016/j.scitotenv.2015.03.008>
- Pfannkuche, J., & Schmidt, A. (2003). Determination of suspended particulate matter concentration from turbidity measurements: Particle size effects and calibration procedures. *Hydrological Processes*, 17(10), 1951–1963. <https://doi.org/10.1002/hyp.1220>
- Rode, M., Wade, A. J., Cohen, M. J., Hensley, R. T., Bowes, M. J., Kirchner, J. W., Arhonditsis, G. B., Jordan, P., Kronvang, B., Halliday, S. J., Skeffington, R. A., Rozemeijer, J. C., Aubert, A. H., Rinke, K., & Jomaa, S. (2016). Sensors in the stream: The high-frequency wave of the present. *Environmental Science & Technology*, 50(19), 10297–10307. <https://doi.org/10.1021/acs.est.6b02155>
- Rose, L. A., Karwan, D. L., & Godsey, S. E. (2018). Concentration–discharge relationships describe solute and sediment mobilization, reaction, and transport at event and longer timescales. *Hydrological Processes*, 32(18), 2829–2844. <https://doi.org/10.1002/hyp.13235>
- Seibert, J., Grabs, T., Köhler, S., Laudon, H., Winterdahl, M., & Bishop, K. (2009). Linking soil-and stream-water chemistry based on a riparian flow-concentration integration model. *Hydrology and Earth System Sciences*, 13(12), 2287–2297.
- Sherriff, S. C., Rowan, J. S., Fenton, O., Jordan, P., Melland, A. R., Mellander, P.-E., & Uallacháin, D. Ó. (2016). Storm event suspended sediment-discharge hysteresis and controls in agricultural watersheds: Implications for watershed scale sediment management. *Environmental Science & Technology*, 50(4), 1769–1778. <https://doi.org/10.1021/acs.est.5b04573>
- Skarbøvik, E., & Roseth, R. (2015). Use of sensor data for turbidity, pH and conductivity as an alternative to conventional water quality monitoring in four Norwegian case studies. *Acta Agriculturae Scandinavica Section B Soil and Plant Science*, 65(1), 63–73. <https://doi.org/10.1080/09064710.2014.966751>
- Stutter, M., Dawson, J. J. C., Glendell, M., Napier, F., Potts, J. M., Sample, J., Vinent, A., & Watson, H. (2017). Evaluating the use of in-situ turbidity measurements to quantify fluvial sediment and phosphorus concentrations and fluxes in agricultural streams. *Science of The Total Environment*, 607–608, 391–402. <https://doi.org/10.1016/j.scitotenv.2017.07.013>
- Swedish Board of Agriculture. *Miljöersättning för skyddszonerna*. (2021.) Available from <https://jordbruksverket.se/stod/lantbruk-skogsbruk-och-trädgård/jordbruksmark/skyddszonerna>
- Swedish Meteorological and Hydrological Institute. *Vattenwebb–Modelldata per område*. (2019). Available from <https://vattenwebb.smhi.se/modelarea/>
- Swedish Meteorological and Hydrological Institute. *Ladda ner meteorologiska observationer | SMHI*. (2020). Available from <https://www.smhi.se/data/meteorologi/ladda-ner-meteorologiska-observatiorer/#param=precipitation24HourSum,stations=all,stationid=97520>
- Tananaev, N. I. (2015). Hysteresis effects of suspended sediment transport in relation to geomorphic conditions and dominant sediment sources in medium and large rivers of the Russian Arctic. *Hydrology Research*, 46(2), 232–243. <https://doi.org/10.2166/nh.2013.199>
- Braak, C. J. F. ter, & Smilauer, P. (2012). *Canoco reference manual and user's guide: Software for ordination, version 5.0*. <https://research.wur.nl/en/publications/canoco-reference-manual-and-users-guide-software-for-ordination-v>
- Ulén, B., & Etana, A. (2014). Phosphorus leaching from clay soils can be counteracted by structure liming. *Acta Agriculturae Scandinavica Section B Soil and Plant Science*, 64(5), 425–433. <https://doi.org/10.1080/09064710.2014.920043>
- van Geer, F. C., Kronvang, B., & Broers, H. P. (2016). High-resolution monitoring of nutrients in groundwater and surface waters: Process understanding, quantification of loads and concentrations, and management applications. *Hydrology and Earth System Sciences*, 20(9), 3619–3629. <https://doi.org/10.5194/hess-20-3619-2016>
- Vercruyse, K., Grabowski, R. C., & Rickson, R. J. (2017). Suspended sediment transport dynamics in rivers: Multi-scale drivers of temporal variation. *Earth-Science Reviews*, 166, 38–52. <https://doi.org/10.1016/j.earscirev.2016.12.016>
- Verstraeten, G., Poelen, J., Gillijns, K., & Govers, G. (2006). The use of riparian vegetated filter strips to reduce river sediment loads: An overestimated control measure? *Hydrological Processes*, 20(20), 4259–4267. <https://doi.org/10.1002/hyp.6155>
- Walling, D. E. (1977). Assessing the accuracy of suspended sediment rating curves for a small basin. *Water Resources Research*, 13(3), 531–538.
- Walling, D. E., & Foster, I. D. L. (1975). Variations in the natural chemical concentration of river water during flood flows, and the lag effect: Some further comments. *Journal of Hydrology*, 26(3–4), 237–244. [https://doi.org/10.1016/0022-1694\(75\)90005-0](https://doi.org/10.1016/0022-1694(75)90005-0)
- Walling, D. E., & Moorehead, P. W. (1987). Spatial and temporal variation of the particle-size characteristics of fluvial suspended sediment. *Geografiska Annaler. Series A, Physical Geography*, 69(1), 47–59.

- Walling, D. E., & Webb, B. W. (1982). Sediment availability and the prediction of storm-period sediment yields. *Recent Developments in the Explanation and Prediction of Erosion and Sediment Yield*, 137, 327–337.
- Wennng, H., Barneveld, R., Bechmann, M., Martila, H., Krogstad, T., & Skarbøvik, E. (2021). Sediment transport dynamics in small agricultural catchments in a cold climate: A case study from Norway. *Agriculture, Ecosystems and Environment*, 317, 107484. <https://doi.org/10.1016/j.agee.2021.107484>
- Williams, G. P. (1989). Sediment concentration versus water discharge during single hydrologic events in rivers. *Journal of Hydrology*, 111(1–4), 89–106. [https://doi.org/10.1016/0022-1694\(89\)90254-0](https://doi.org/10.1016/0022-1694(89)90254-0)
- Wymore, A. S., Leon, M. C., Shanley, J. B., & McDowell, W. H. (2019). Hysteretic response of solutes and turbidity at the event scale across forested tropical montane watersheds. *Frontiers in Earth Science*, 7(126). <https://doi.org/10.3389/feart.2019.00126>
- Ziegler, A. D., Benner, S. G., Tantasirin, C., Wood, S. H., Sutherland, R. A., Sidle, R. C., Jachowski, N., Nullet, M. A., Xi, L. X., Snidvongs, A., Giambelluca, T. W., & Fox, J. M. (2014). Turbidity-based sediment monitoring in northern Thailand: Hysteresis, variability, and uncertainty. *Journal of Hydrology*, 519, 2020–2039. <https://doi.org/10.1016/j.jhydrol.2014.09.010>

## SUPPORTING INFORMATION

Additional supporting information may be found in the online version of the article at the publisher's website.

**How to cite this article:** Lannerård, E. E., Fölster, J., & Futter, M. N. (2021). Turbidity-discharge hysteresis in a meso-scale catchment: The importance of intermediate scale events. *Hydrological Processes*, 35(12), e14435. <https://doi.org/10.1002/hyp.14435>